

High-Q magnetic levitation and control of superconducting microspheres at millikelvin temperatures

J. Hofer,^{1, 2, *} G. Higgins,^{2, 3} H. Huebl,^{4, 5, 6} O. F. Kieler,⁷ R. Kleiner,⁸ D. Koelle,⁸ P. Schmidt,² J. A. Slater,^{1, †} M. Trupke,¹ K. Uhl,⁸ T. Weimann,⁷ W. Wieczorek,^{1, 3} F. Wulschner,¹ and M. Aspelmeyer^{1, 2}

¹University of Vienna, Faculty of Physics, Vienna Center for Quantum Science and Technology (VCQ), A-1090 Vienna, Austria

²Institute for Quantum Optics and Quantum Information (IQOQI),

Austrian Academy of Sciences, A-1090 Vienna, Austria

³Department of Microtechnology and Nanoscience (MC2),

Chalmers University of Technology, S-412 96 Gothenburg, Sweden

⁴Walther-Meissner-Institut, Bayerische Akademie der Wissenschaften, D-85748 Garching, Germany

⁵Physik-Department, Technische Universität München, D-85748 Garching, Germany

⁶Munich Center for Quantum Science and Technology (MCQST), D-80799 München, Germany

⁷Physikalisch-Technische Bundesanstalt (PTB), D-38116 Braunschweig, Germany

⁸Physikalisches Institut, Center for Quantum Science (CQ) and LISA⁺,

University of Tuebingen, D-72076 Tuebingen, Germany

(Dated: November 14, 2022)

We report the levitation of a superconducting lead-tin sphere with 100 μm diameter (corresponding to a mass of 5.6 μg) in a static magnetic trap formed by two coils in an anti-Helmholtz configuration, with adjustable resonance frequencies up to 240 Hz. The center-of-mass motion of the sphere is monitored magnetically using a dc-SQUID as well as optically and exhibits quality factors of up to 2.6×10^7 . We also demonstrate 3D magnetic feedback control of the sphere's motion. By implementing a cryogenic vibration isolation system we can attenuate environmental vibrations at 200 Hz by approximately seven orders of magnitude. The combination of low temperature (15 mK), large mass and high quality factor as well as adjustable resonance frequencies provides a promising platform for testing quantum physics in previously unexplored regimes with high mass and long coherence times.

Diamagnets and superconductors partially expel magnetic fields, allowing stable levitation in field minima [1]. A prominent application of magnetically levitated systems is the use as ultra-precise acceleration sensors, most notably in the superconducting gravimeter [2], which relies on the levitation of centimeter-sized hollow superconducting spheres in a stable magnetic field generated by superconducting coils in persistent current mode. More recently, several proposals [3, 4] have highlighted the potential of magnetic levitation for tests of quantum physics with macroscopic, micrometer-sized objects.

Successfully preparing a magnetically levitated particle in a quantum state requires a magnetic trap with low damping, low heating rates and the ability to control the mechanical motion. Some of these features are already present in recent demonstrations of magnetically levitated systems, such as the levitation of permanent magnets above a superconducting surface [5, 6] and the levitation of diamagnets in the field of permanent magnets at cryogenic temperatures [7] or room temperature [8]. However, as of yet no system has combined these features. Furthermore, as typical levitation frequencies for these systems range from sub-hertz to kilohertz, the heating rate is dominated by environmental vibrations.

One of the most promising avenues towards the quantum regime is the levitation of a type-I (or zero-field-cooled type-II) superconductor in a magnetic field produced by persistent currents, as this avoids dissipation due to hysteresis and eddy currents, which is inherent to

levitation schemes involving ferromagnets or flux-pinned type-II superconductors [9, 10]. The only remaining dissipation mechanisms are expected to be collisions with residual gas particles and blackbody radiation interactions [3] as well as the movement of residual unpaired electrons inside the superconductor [11], all of which are minimized at low temperatures. Using persistent currents should result in an extremely stable trap, as both the drift and noise can be kept extremely low [2, 12, 13]. Working at millikelvin temperatures also naturally enables coupling to non-linear quantum systems such as superconducting qubits [3], and miniaturizing the trap architecture [14–16] might lead to fully on-chip coupled quantum systems [17]. In comparison with optical levitation, which has already been established as a means to study massive objects in the quantum regime [18–20], magnetostatic levitation has the potential to access a new parameter regime of even larger mass and longer coherence times [3, 21]: While the size of optically levitated particles is in practice limited by the available laser power to the micrometer scale [22], magnetic levitation can support train-scale objects [23] and due to the static nature of the fields there is no decoherence due to photon recoil or absorption.

A first step towards a fully superconducting platform was presented in [24], where a lead particle was levitated in the magnetic field of a superconducting coil. This approach, however, was limited in performance by the presence of cryogenic exchange gas at 4 K and environmental

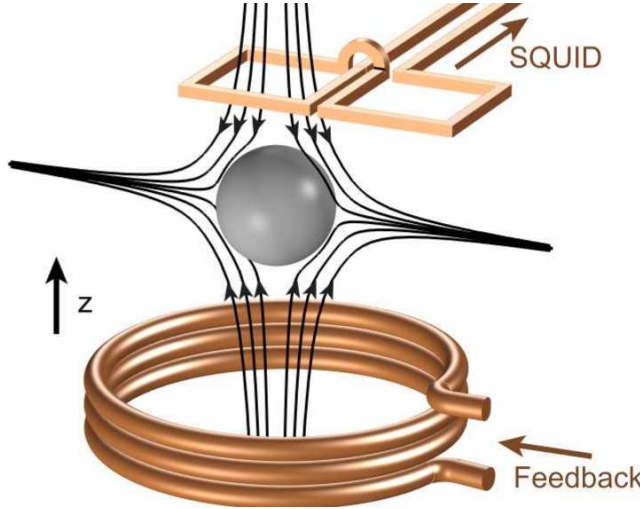


FIG. 1. Conceptual representation of the experiment showing the levitated sphere, the pickup coil and the feedback coil. The trap field is depicted by its field lines.

vibrations. Here we report an experiment that provides orders of magnitude improvements in both damping and vibration isolation. We demonstrate the levitation of a superconducting sphere in the magnetic field generated by a superconducting coil. We detect the particle's center of mass (COM) motion magnetically by inductive coupling to a superconducting quantum interference device (SQUID) via a pickup coil (cf. Fig. 1) and demonstrate feedback control of all three COM translational degrees of freedom by real-time processing of the SQUID signal. We find that the motion of the particle has a low damping rate, corresponding to quality factors of up to 2.6×10^7 . We also implement a custom vibration isolation system to reduce heating from environmental vibrations. Finally, we discuss the limitations of our current setup and the improvements that are necessary for ground state cooling.

Trapping.— The energy of an object of volume V with permeability μ in an applied magnetic field B_0 in free space can be approximated by $-1/2V(\mu - \mu_0)B_0^2$ [1], where μ_0 is the permeability of free space. Because $\nabla^2 B_0^2 \geq 0$, stable levitation is possible in a field minimum for $\mu < \mu_0$, i.e. for diamagnets. A superconducting sphere can act as a perfect diamagnet ($\mu = 0$), because it reacts to a change in the applied magnetic field by forming screening currents on its surface, counteracting the applied field and keeping the interior of the sphere field-free. This behavior occurs for type-I superconductors and zero-field-cooled type-II superconductors, provided the applied field strength on the surface of the superconductor stays below a material-dependent maximum value at all times [11].

For a sphere trapped in the field of an anti-Helmholtz coil, the resulting potential close to the field minimum

is harmonic and two of the COM modes are degenerate [3, 25]. To lift the degeneracy we use elliptical coils; each coil has a cross section of $5 \text{ mm} \times 6 \text{ mm}$ and the coils are separated by approximately 4.5 mm . The z -direction is along the coil axis, which coincides with the vertical direction, while x and y are perpendicular to z , with x along the major axis of the elliptical coils. We use numerical simulations [26] to model the magnetic field created by such an arrangement and confirm that the magnetic field near the center between the coils is well-described by $(b_x x, b_y y, b_z z)$, where the field gradients b_i are proportional to the trap current with $|b_x| < |b_y| < |b_z|$ and $b_z = -(b_x + b_y)$. This field shape constitutes a three-dimensional harmonic trap for a levitated superconducting sphere with the COM frequencies [26]

$$f_i = \sqrt{\frac{3}{8\pi^2 \mu_0 \rho}} |b_i|, \quad (1)$$

where ρ is the sphere's density.

Our setup is housed in a dilution refrigerator (Bluefors BF-LD400) with a loaded base temperature of approximately 15 mK . The microspheres are commercial (Easy-Spheres) solder balls with diameter $100(6) \text{ }\mu\text{m}$, made of a 90-10 lead-tin alloy with density $\rho = 10.9 \times 10^3 \text{ kg/m}^3$. Lead-tin is a type-II superconductor with a critical temperature of approximately 7 K [27]. A single sphere is initially placed in a 3D-printed polylactide bowl glued to the lower trap coil, such that it rests around 1 mm below the trap center. The bowl helps to prevent accidental loss of the sphere during assembly and between measurement runs. After cooling down the system to millikelvin temperatures, lift-off is achieved by increasing the coil current until the upward magnetic force on the sphere is stronger than the downward gravitational and adhesive forces. The trap coils are surrounded by an aluminum shield with small openings for optical access and wires, which screens the sphere from magnetic field fluctuations when the aluminum is superconducting. Numerical simulations predict a screening factor of more than 1×10^6 at the trap center. To suppress field fluctuations from the trapping coils and feedback coil, we use a low pass filter and attenuation stages, respectively [26]. No normal conductors are present inside the shield as currents induced in them due to the motion of the sphere would cause dissipation (eddy current damping).

Readout.— A planar Niobium thin film gradiometric pickup coil consisting of two square loops positioned approximately $400 \text{ }\mu\text{m}$ above the trap center is used to magnetically probe the particle motion. Each loop is $145 \text{ }\mu\text{m} \times 145 \text{ }\mu\text{m}$ and the separation between the loops is $3 \text{ }\mu\text{m}$. As the particle moves, it induces a current in the pickup loop [26], which is connected with Nb wires to the input coil of a SQUID current sensor [28]. The SQUID has an intrinsic flux noise level of $S_\Phi^{1/2} = 0.8 \text{ }\mu\Phi_0/\sqrt{\text{Hz}}$, where $\Phi_0 \approx 2.1 \times 10^{-15} \text{ Wb}$ is the flux quantum. When

the SQUID is incorporated into the setup and the pickup loop is connected, the noise rises to $S_\Phi^{1/2} \approx 10 \mu\Phi_0/\sqrt{\text{Hz}}$. We believe this is due to external field fluctuations inductively coupling into the wires connecting the pickup loop and the SQUID. With a commercial SQUID (Supracon CSblue), that was used for some of the measurements, the noise floor in the setup further increased by an order of magnitude.

To calibrate the SQUID signal we optically record the sphere's motion by illuminating it and imaging its shadow on a camera, while simultaneously recording the motion with the SQUID [26]. The coupling strengths (flux induced in the SQUID per sphere displacement) for the different motional modes depend on the position of the pickup loop in relation to the sphere as well as the trap gradients, i.e. mechanical frequencies. The highest measured coupling strength was approximately $13 \times 10^3 \Phi_0/\text{m}$ for the z -mode and $3 \times 10^3 \Phi_0/\text{m}$ for the x - and y -modes. Together with a flux noise floor of $10 \mu\Phi_0/\sqrt{\text{Hz}}$ these coupling strengths correspond to a displacement sensitivity of approximately $1 \text{ nm}/\sqrt{\text{Hz}}$ for the z -mode. During these measurements the separation between pickup loop and sphere was approximately $400 \mu\text{m}$. We estimate that with a smaller separation and an optimized pickup loop geometry an improvement of four orders of magnitude is possible [26].

Mechanical frequencies.— The particle's COM frequencies are visible in the power spectral density of the SQUID signal, as shown in Fig. 2. The COM frequencies depend linearly on the trap's magnetic field gradient (see Eq. 1) and thus the current in the trap coils, as shown in the inset. The highest frequency reached in the present setup is 240 Hz (corresponding to $b_z \approx 150 \text{ T/m}$), limited by the maximum current output of the low-noise current source. We can trap at lower frequencies, down to $f_z \approx 20 \text{ Hz}$, where the lower limit stems from the gravity-induced shift of the trapping position and our trap geometry. However, at low trapping frequencies the sphere is strongly excited by environmental vibrations.

Feedback.— We can apply a magnetic feedback force on the levitated sphere by processing the SQUID signal and applying a feedback current to a small coil with approximately 20 windings positioned approximately 1 mm below the trap center. The feedback current modifies the field strength as well as the field gradient at the trap center, enabling us to apply direct and parametric feedback, respectively. Since the COM modes are separated in frequency, we can apply feedback to all modes simultaneously. To apply direct feedback we pass the SQUID signal to a FPGA (STEMlab 125-14), which applies a bandpass-filter, gain and phase shift [29], before feeding the signal to the feedback coil. For parametric feedback at twice the mechanical frequencies we use a phase-locked loop and a clock divider on a second FPGA. Our feedback scheme is currently limited by measurement noise rather than thermal noise. As this prevents cooling be-

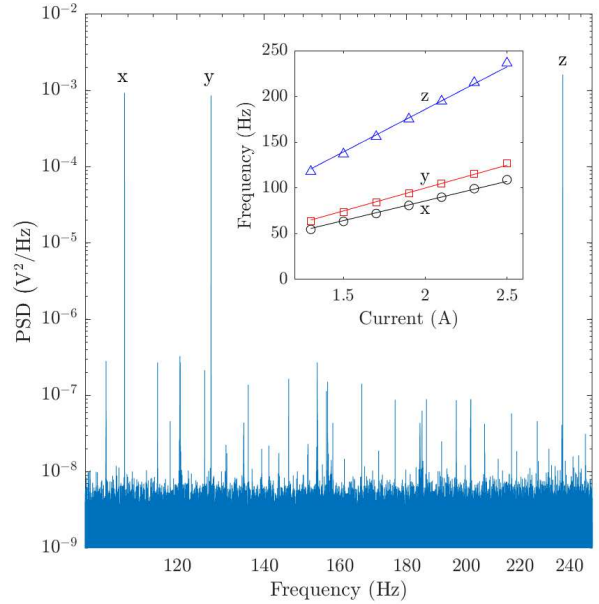


FIG. 2. The power spectral density of the SQUID signal displays three peaks which correspond to the particle's COM modes. The particle's motion is excited to approximately one micrometer rms displacement in this figure - measurement noise prevents us from resolving the equilibrium motion of the particle. The inset shows the linear dependence of the COM frequencies on the trap current. The solid lines are zero-intercept linear fits.

low the equilibrium temperature of the COM modes, we use feedback here only as a means to quickly adjust the amplitudes and prepare other measurements (cf. Fig. 3, inset).

Quality factor.— We measure the quality factor by performing ringdown measurements. We extract the quality factor from an exponential fit to the measured amplitude, where the initial starting amplitude is set by applying an appropriate feedback signal before the start of the measurement. We do see occasional jumps in the damping rate (cf. Fig. 3), which we attribute to the detaching and attaching of flux lines to a pinning center. Unpinned flux lines can move within the superconductor (flux creep), a mechanism that is known to cause damping in the levitation of flux-pinned superconductors or magnets [10, 30]. Although we do not apply a magnetic field during the cooldown, there is a non-zero background field and hence we expect some frozen-in flux to be present in the levitated sphere. As a consequence, the measured quality factors vary with time and between measurement runs, but they are generally between 1×10^7 and 2.5×10^7 for the z -mode and about half as high for the x - and y -modes. The highest quality factor we have measured is 2.6×10^7 at 212 Hz, corresponding to a dissipation rate of $5 \times 10^{-5} \text{ s}^{-1}$ and likely still limited by flux

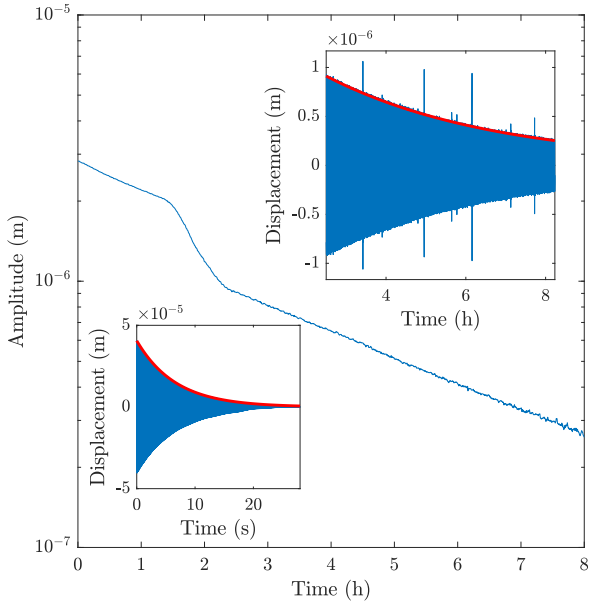


FIG. 3. Ringdown measurement of the z-mode. The upper right inset shows a linear plot for the latter part of the data, starting at $t=2.5$ h. The red line is a fit to an exponential decay. The spikes correspond to a brief loss of the SQUID lock, they were removed for the amplitude plot. The lower left inset shows a ringdown while direct feedback is applied (note that the x-axis scale is in seconds).

creep inside the particle. We also consider other possible contributions to the damping [26], but find that the expected contributions cannot explain the measured values. In future experiments we plan to use a particle made of a type-I superconductor such as mono-crystalline lead, which will expel all magnetic flux via the Meissner effect and prevent flux creep. Alternatively, pinned flux inside the sphere could also be avoided by the use of ferromagnetic shields.

Sensing.— A massive system acting as a harmonic oscillator can be used for force and acceleration sensing, with the sensitivities depending on the mass m and the dissipation rate γ of the oscillator. In equilibrium with a thermal bath at temperature T_0 , the thermal force noise is given by $\sqrt{S_{FF}^{\text{th}}} = \sqrt{4k_B T_0 m \gamma}$ [31], where k_B is Boltzmann's constant. The dissipation rate γ is related to the quality factor Q and the angular mechanical resonance frequency ω_0 by $\gamma = \omega_0/Q$. The corresponding acceleration sensitivity is $\sqrt{S_{FF}^{\text{th}}}/m$. For a particle of mass $m \approx 5.6 \mu\text{g}$ in thermal equilibrium with the surroundings in the dilution refrigerator at 15 mK, this sets the limits for force and acceleration sensing at $5 \times 10^{-19} \text{ N}/\sqrt{\text{Hz}}$ and $9 \times 10^{-12} \text{ g}/\sqrt{\text{Hz}}$, using our highest measured quality factor $Q = 2.6 \times 10^7$ at 212 Hz. We can also use our setup to measure vibrations and magnetic field fluctuations, each

of which cause displacement of the trap center and therefore excite the oscillator. Using the same parameters as above, the thermally-limited vibration and magnetic field fluctuation sensitivities are $5 \times 10^{-17} \text{ m}/\sqrt{\text{Hz}}$ and $6 \times 10^{-15} \text{ T}/\sqrt{\text{Hz}}$, respectively (for vibrations and magnetic field fluctuations along the z-axis). Our current experimental sensitivities are approximately one order of magnitude above the thermal noise, limited by drifts in the trap current and measurement noise [26].

Cryogenic vibration isolation.— Vibrations of the cryostat accelerate the trapping coils and thus the trap center, effecting a force onto the levitated sphere. Denoting the vibrational power spectral density by $S_{\epsilon\epsilon}$ and including thermal noise, the displacement power spectral density of our sphere is given as

$$S_{zz}(\omega) = |\chi(\omega)|^2 [4k_B T_0 m \gamma + m^2 \omega_0^4 S_{\epsilon\epsilon}(\omega)],$$

where χ denotes the mechanical susceptibility. On resonance, above the thermal noise, this reduces to $\sqrt{S_{zz}} \approx Q\sqrt{S_{\epsilon\epsilon}}$. From independent accelerometer measurements on the cryostat we estimate $\sqrt{S_{\epsilon\epsilon}} \approx 1 \times 10^{-10} \text{ m}/\sqrt{\text{Hz}}$ at 200 Hz, which would result in a peak height of $2.6 \times 10^{-3} \text{ m}/\sqrt{\text{Hz}}$ and a root-mean-square displacement of approximately 9 μm , corresponding to an effective temperature $T_{\text{eff}} \approx 6 \times 10^{10} \text{ K}$. To mitigate the effects of vibrations we implement a passive cryogenic vibration isolation system: the aluminum shield containing the trap is hung from the 4 K-stage of the dilution refrigerator via 38 μm -thick stainless steel wires and two intermediate stages. The system acts like a triple pendulum, offering isolation from horizontal (x and y) vibrations, while the elasticity of the wires provides isolation from vertical (z) vibrations. To prevent coupling of external vibrations into the experimental setup via electrical wires and the copper braids used for thermalization, we connect these wires and braids to an additional vibration isolation platform, as represented in Fig. 4. Vibrations of the experimental system could also be induced by fluctuating magnetic fields acting on the aluminum shield. To prevent this, we surround the setup by a second aluminum shield which is rigidly mounted to the cryostat. We typically operate at vertical (z) trap frequencies above 200 Hz and initially found that the vibration isolation system attenuates vibrations at these frequencies by approximately five orders of magnitude. We have further improved the system by optimizing the mass and wire length for each stage, leading to an attenuation of almost seven orders of magnitude at 200 Hz. Theoretically, vibrations along the horizontal axis as well as librational fluctuations around the axes are suppressed even more, but in practice we expect vibrations from the vertical axis to couple into all degrees of freedom [32]. More details on the vibration isolation platform are provided in [26].

Prospects for ground state cooling.— We now discuss the potential of this system to reach the ground state, which would be a first step towards accessing

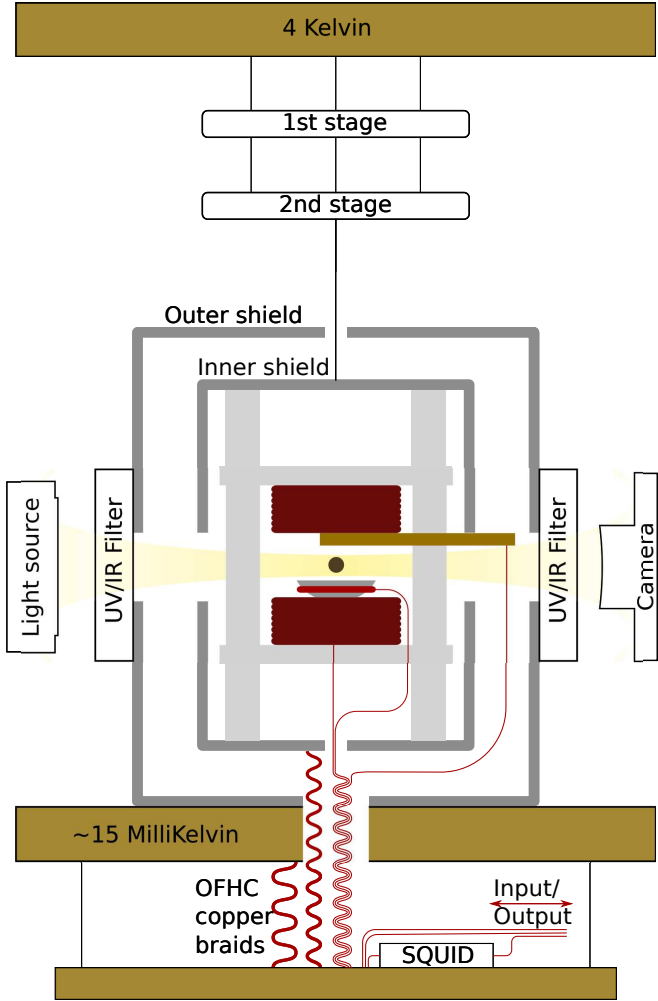


FIG. 4. Sketch of the setup including the vibration isolation system (not to scale). The light source is turned on only for calibration measurements. The UV/IR cutoff filters on the millikelvin stage prevent ambient radiation from heating the levitated sphere.

the quantum regime. SQUID noise can be separated into flux noise $S_{\phi\phi}$ and noise in the circulating current S_{JJ} , which may be partially correlated [33] and fulfill $\sqrt{S_{\phi\phi}S_{JJ}} - S_{\phi J}^2 \geq \hbar$ [34, 35]. The flux noise results in the measurement noise $\frac{S_{\phi\phi}}{\eta^2}$, while the current noise corresponds to a back action $\eta^2 S_{JJ}$, where η is the coupling strength. Applying direct feedback with optimum gain and assuming vanishing correlations between flux and current noise, one can estimate the final phonon occupation [26] as

$$\bar{n} = \frac{1}{\hbar\eta^2} \left(2k_B T_0 m \gamma \tilde{L}_S \right) + \frac{1}{2} \left(\frac{\sqrt{S_{\phi\phi}S_{JJ}}}{\hbar} - 1 \right),$$

where $\tilde{L}_S = \sqrt{\frac{S_{\phi\phi}}{S_{JJ}}}$ depends on the working point of the SQUID and is typically on the order of the SQUID

inductance L_S . The first term describes heating from coupling to an effective thermal reservoir with temperature T_0 , while the second term is the back-action limit under continuous feedback. We can reach a coupling strength of $\eta \approx 5 \times 10^7 \phi_0/m$ [26], so for $T_0 \approx 15 \text{ mK}$ and a typical SQUID inductance of $L_S \approx 15 \text{ pH}$ we need $\gamma \approx 1 \times 10^{-6} \text{ s}^{-1}$ to keep the former negligible. Ground state cooling then requires $\sqrt{S_{\phi\phi}S_{JJ}} < 3\hbar$. In addition to feedback cooling with a SQUID, we will investigate other potential avenues for ground state cooling such as coupling the levitated sphere to a flux qubit or a microwave cavity [3].

Discussion and outlook.— We built a platform based on the diamagnetic levitation of a superconductor in a magnetostatic trap at 15 mK and demonstrate quality factors exceeding 1×10^7 for the three COM modes of a 5.6 μg oscillator. The high quality factors result in excellent sensing capabilities, with achievable force (acceleration) sensitivities that are otherwise only reached with much smaller (larger) masses [2, 36]. We also demonstrated simultaneous feedback cooling of all COM modes using either direct or parametric feedback. While we have focused here on a 100 μm -sized sphere, the setup allows for particles from sub-micron size to millimeter size to be levitated [25]. We have identified improvements to mitigate technical issues: First, we plan to use a type-I superconducting sphere to avoid trapped flux and dissipation caused by flux creep, which we expect is limiting our quality factor. Second, we can improve the magnetomechanical coupling by four orders of magnitude by better positioning of the pickup coil and by using a pickup coil with multiple windings matched to the input coil of the SQUID. Together with an optimized SQUID shielded from environmental noise (s.t. our readout is limited by the intrinsic SQUID noise) this would result in an improvement of the measurement noise floor by six orders of magnitude [26]. Third, we plan to implement a persistent current switch to improve the trap current stability. Additionally, we will explore coupling to a SQUID-terminated microwave-resonator [37–39] to access the toolbox of circuit QED. With these improvements, our system offers a promising approach for bringing microgram objects to the quantum regime, which opens a potential avenue for quantum-limited acceleration sensing or even probing quantum effects of gravity [40–43].

We thank G. Kirchmair, O. Romero-Isart and A. Sanchez for discussions, and R. Gross for discussions as well as providing us access to the infrastructure of the Walther-Meissner-Institute for low temperature research in Garching during the initial phase of the project. We also thank Matthias Rudolph for assisting with the initial setup of a SQUID measurement system. This work was supported by the European Union's Horizon 2020 research and innovation programme under grant agreement No 863132 (iQLev), the European Union's Horizon

Europe 2021-2027 Framework Programme under grant agreement No 101080143 (SuperMeQ), the European Research Council (ERC CoG QLev4G and ERC Synergy QXtreme), and the Austrian Science Fund (FWF) under project F40 (SFB FOQUS). We gratefully acknowledge financial support from the Deutsche Forschungsgemeinschaft (DFG, German Research Foundation) under Germany's Excellence Strategy – EXC-2111 – 390814868. G. Higgins acknowledges support from the Swedish Research Council (grant no. 2020-00381). P. Schmidt is supported by the Alexander von Humboldt Foundation through a Feodor Lynen Fellowship.

* joachim.hofer@univie.ac.at

† Currently at: QuTech, Delft University of Technology, Delft, The Netherlands

- [1] E. H. Brandt, Levitation in physics, *Science* **243**, 349 (1989).
- [2] J. M. Goodkind, The superconducting gravimeter, *Review of Scientific Instruments* **70**, 4131 (1999).
- [3] O. Romero-Isart, L. Clemente, C. Navau, A. Sanchez, and J. I. Cirac, Quantum magnetomechanics with levitating superconducting microspheres, *Phys. Rev. Lett.* **109**, 147205 (2012).
- [4] M. Cirio, G. K. Brennen, and J. Twamley, Quantum magnetomechanics: Ultrahigh- q -levitated mechanical oscillators, *Phys. Rev. Lett.* **109**, 147206 (2012).
- [5] A. Vinante, P. Falferi, G. Gasbarri, A. Setter, C. Timberlake, and H. Ulbricht, Ultralow mechanical damping with meissner-levitated ferromagnetic microparticles, *Phys. Rev. Appl.* **13**, 101103/PhysRevApplied.13.064027 (2020).
- [6] J. Gieseler, A. Kabcenell, E. Rosenfeld, J. D. Schaefer, A. Safira, M. J. A. Schuetz, C. Gonzalez-Ballester, C. C. Rusconi, O. Romero-Isart, and M. D. Lukin, Single-spin magnetomechanics with levitated micromagnets, *Phys. Rev. Lett.* **124**, 163604 (2020).
- [7] Y. Leng, R. Li, X. Kong, H. Xie, D. Zheng, P. Yin, F. Xiong, T. Wu, C.-K. Duan, Y. Du, Z.-q. Yin, P. Huang, and J. Du, Mechanical dissipation below 1 μ Hz with a cryogenic diamagnetic levitated micro-oscillator, *Phys. Rev. Applied* **15**, 024061 (2021).
- [8] C. W. Lewandowski, T. D. Knowles, Z. B. Etienne, and B. D'Urso, High-sensitivity accelerometry with a feedback-cooled magnetically levitated microsphere, *Phys. Rev. Applied* **15**, 014050 (2021).
- [9] T. Wang, S. Lourette, S. R. O'Kelley, M. Kayci, Y. Band, D. F. J. Kimball, A. O. Sushkov, and D. Budker, Dynamics of a ferromagnetic particle levitated over a superconductor, *Phys. Rev. Applied* **11**, 044041 (2019).
- [10] E. H. Brandt, Friction in levitated superconductors, *Applied Physics Letters* **53**, 1554 (1988).
- [11] M. Tinkham, *Introduction to Superconductivity* (Dover Publications, 1996).
- [12] R. S. Van Dyck, D. L. Farnham, S. L. Zafonte, and P. B. Schwinberg, Ultrastable superconducting magnet system for a penning trap mass spectrometer, *Review of Scientific Instruments* **70**, 1665 (1999).
- [13] J. W. Britton, J. G. Bohnet, B. C. Sawyer, H. Uys, M. J. Biercuk, and J. J. Bollinger, Vibration-induced field fluctuations in a superconducting magnet, *Phys. Rev. A* **93**, 062511 (2016).
- [14] M. G. Latorre, J. Hofer, M. Rudolph, and W. Wieczorek, Chip-based superconducting traps for levitation of micrometer-sized particles in the meissner state, *Superconductor Science and Technology* **33**, 105002 (2020).
- [15] M. G. Latorre, A. Paradkar, D. Hambraeus, G. Higgins, and W. Wieczorek, A chip-based superconducting magnetic trap for levitating superconducting microparticles, *IEEE Transactions on Applied Superconductivity* **32**, 1 (2022).
- [16] M. G. Latorre, G. Higgins, A. Paradkar, T. Bauch, and W. Wieczorek, Superconducting microsphere magnetically levitated in an anharmonic potential (2022), arXiv:2210.13451 [quant-ph].
- [17] H. Pino, J. Prat-Camps, K. Sinha, B. P. Venkatesh, and O. Romero-Isart, On-chip quantum interference of a superconducting microsphere, *Quantum Science and Technology* **3**, 025001 (2018).
- [18] U. Delic, M. Reisenbauer, K. Dare, D. Grass, Vuletic Vladan, N. Kiesel, and M. Aspelmeyer, Cooling of a levitated nanoparticle to the motional quantum ground state, *Science* **367**, 892 (2020).
- [19] L. Magrini, P. Rosenzweig, C. Bach, A. Deutschmann-Olek, S. G. Hofer, S. Hong, N. Kiesel, A. Kugi, and M. Aspelmeyer, Real-time optimal quantum control of mechanical motion at room temperature, *Nature* **595**, 373 (2021).
- [20] F. Tebbenjohanns, M. L. Mattana, M. Rossi, M. Frimmer, and L. Novotny, Quantum control of a nanoparticle optically levitated in cryogenic free space, *Nature* **595**, 378 (2021).
- [21] C. Navau, S. Minniberger, M. Trupke, and A. Sanchez, Levitation of superconducting microrings for quantum magnetomechanics, *Phys. Rev. B* **103**, 174436 (2021).
- [22] F. Monteiro, S. Ghosh, A. G. Fine, and D. C. Moore, Optical levitation of 10- μ m spheres with nano- g acceleration sensitivity, *Phys. Rev. A* **96**, 063841 (2017).
- [23] P.-Z. C. Francis C. Moon, *Superconducting Levitation: Applications to Bearings and Magnetic Transportation* (Wiley-VCH, 1995).
- [24] B. van Waarde, *The lead zeppelin : a force sensor without a handle*, Ph.D. thesis, Leiden University (2016).
- [25] J. Hofer and M. Aspelmeyer, Analytic solutions to the maxwell-london equations and levitation force for a superconducting sphere in a quadrupole field, *Physica Scripta* **94**, 125508 (2019).
- [26] See supplemental material below for more information on the derivation of trap parameters, the effects of trap current fluctuations, the vibration isolation system, estimations of different contributions to the damping, the calibration of the squid signal as well as more details on ground state cooling.
- [27] J. D. Livingston, Magnetic properties of superconducting lead-base alloys, *Phys. Rev.* **129**, 1943 (1963).
- [28] J.-H. Storm, O. Kieler, and R. Körber, Towards ultrasensitive squids based on submicrometer-sized josephson junctions, *IEEE Transactions on Applied Superconductivity* **30**, 1 (2020).
- [29] L. Neuhaus, R. Metzdorff, S. Chua, T. Jacqmin, T. Britant, A. Heidmann, P.-F. Cohadon, and S. Deléglise, Pyrpl (python red pitaya lockbox) — an open-source

software package for fpga-controlled quantum optics experiments, in *2017 Conference on Lasers and Electro-Optics Europe European Quantum Electronics Conference (CLEO/Europe-EQEC)* (2017) pp. 1–1.

[30] V. V. Nemoshkalenko, E. H. Brandt, A. A. Kordyuk, and B. G. Nikitin, Dynamics of a permanent magnet levitating above a high-*T_c* superconductor, *Physica C* **170**, 481–485 (1990).

[31] R. Kubo, The fluctuation-dissipation theorem, *Reports on Progress in Physics* **29**, 255 (1966).

[32] T. L. Aldcroft, P. F. Michelson, R. C. Taber, and F. A. McLoughlin, Six-degree-of-freedom vibration isolation systems with application to resonant-mass gravitational radiation detectors, *Review of Scientific Instruments* **63**, 3815 (1992).

[33] C. D. Tesche and J. Clarke, dc squid: Current noise, *Journal of Low Temperature Physics* **37**, 397 (1979).

[34] R. H. Koch, D. J. Van Harlingen, and J. Clarke, Quantum noise theory for the dc squid, *Applied Physics Letters* **38**, 380 (1981).

[35] V. Danilov, K. Likharev, and A. Zorin, Quantum noise in squids, *IEEE Transactions on Magnetics* **19**, 572 (1983).

[36] D. Hempston, J. Vovrosh, M. Toroš, G. Winstone, M. Rashid, and H. Ulbricht, Force sensing with an optically levitated charged nanoparticle, *Applied Physics Letters* **111**, 133111 (2017).

[37] P. Schmidt, M. T. Amawi, S. Pogorzalek, F. Deppe, A. Marx, R. Gross, and H. Huebl, Sideband-resolved resonator electromechanics based on a nonlinear josephson inductance probed on the single-photon level, *Communications Physics* **3**, 233 (2020).

[38] O. Shevchuk, G. A. Steele, and Y. M. Blanter, Strong and tunable couplings in flux-mediated optomechanics, *Phys. Rev. B* **96**, 014508 (2017).

[39] D. Zoepfl, M. L. Juan, C. M. F. Schneider, and G. Kirchmair, Single-photon cooling in microwave magnetomechanics, *Phys. Rev. Lett.* **125**, 023601 (2020).

[40] S. P. Kumar and M. B. Plenio, On quantum gravity tests with composite particles, *Nature Communications* **11**, 3900 (2020).

[41] C. Marletto and V. Vedral, Gravitationally induced entanglement between two massive particles is sufficient evidence of quantum effects in gravity, *Phys. Rev. Lett.* **119**, 240402 (2017).

[42] S. Bose, A. Mazumdar, G. W. Morley, H. Ulbricht, M. Toroš, M. Paternostro, A. A. Geraci, P. F. Barker, M. S. Kim, and G. Milburn, Spin entanglement witness for quantum gravity, *Phys. Rev. Lett.* **119**, 240401 (2017).

[43] M. Aspelmeyer, How to avoid the appearance of a classical world in gravity experiments (2022), arXiv:2203.05587 [quant-ph].

Supplemental material: High-Q magnetic levitation and control of superconducting microspheres at millikelvin temperatures

J. Hofer,^{1, 2, *} G. Higgins,^{2, 3} H. Huebl,^{4, 5, 6} O. F. Kieler,⁷ R. Kleiner,⁸ D. Koelle,⁸ P. Schmidt,² J. A. Slater,^{1, †} M. Trupke,¹ K. Uhl,⁸ T. Weimann,⁷ W. Wieczorek,^{1, 3} F. Wulschner,¹ and M. Aspelmeyer^{1, 2}

¹University of Vienna, Faculty of Physics, Vienna Center for Quantum Science and Technology (VCQ), A-1090 Vienna, Austria

²Institute for Quantum Optics and Quantum Information (IQOQI),

Austrian Academy of Sciences, A-1090 Vienna, Austria

³Department of Microtechnology and Nanoscience (MC2),

Chalmers University of Technology, S-412 96 Gothenburg, Sweden

⁴Walther-Meissner-Institut, Bayerische Akademie der Wissenschaften, D-85748 Garching, Germany

⁵Physik-Department, Technische Universität München, D-85748 Garching, Germany

⁶Munich Center for Quantum Science and Technology (MCQST), D-80799 München, Germany

⁷Physikalisch-Technische Bundesanstalt (PTB), D-38116 Braunschweig, Germany

⁸Physikalisches Institut, Center for Quantum Science (CQ) and LISA⁺,

University of Tuebingen, D-72076 Tuebingen, Germany

(Dated: November 14, 2022)

We provide more information on: (i)The field distribution of the magnetic trap, the resulting trap frequencies and the derivation of the coupling strength. (ii)Effects of current fluctuations and drifts on the measured spectral density. (iii)Limits to the force sensitivity due to measurement noise and current drifts. (iv)The vibration isolation system. (v)Possible contributions to the damping. (vi)Calibration of the SQUID signal. (vii)Optimizations and requirements for ground state cooling.

DERIVATION OF THE MAGNETIC TRAP'S PROPERTIES

Trapping field

We performed numerical simulations in COMSOL MULTIPHYSICS to predict the field configuration generated by the arrangement of our trapping coils. The design of the coils and the simulated magnetic field density are shown in Fig. 1a,b. The field gradients for a trap current of 2.5 A are obtained as $(b_x, b_y, b_z) = (57, 90, 147) \text{ T/m}$, which would correspond to frequencies of (92, 144, 236)Hz. Comparing this to the measured values of (109, 127, 236)Hz we can see that the agreement between the numerical and measured z-mode frequency is excellent, but that the simulations predict a much stronger split for the x- and y-mode than what we see in the experiment. This is likely due to the fact that the spooling process resulted in coils that were more circular than the design (cf. Fig. 1c). For a perfectly circular coil the x- and y-mode frequencies are degenerate [1], so a smaller frequency split is to be expected. Close to the center the field is very well approximated by a quadrupole field: Within a cubic volume of $200 \mu\text{m} \times 200 \mu\text{m} \times 200 \mu\text{m}$ the maximum relative root-mean-square deviation, defined as $|\mathbf{B}_{\text{sim}} - (b_x x, b_y y, b_z z)|/|\mathbf{B}_{\text{sim}}|$, is less than 0.1 %.

Mechanical frequencies

In this section we build on the calculations in [1] to analytically calculate the magnetic field distribution for a superconducting sphere in an axially-asymmetric magnetic

quadrupole field. We consider a superconducting sphere at the origin of the coordinate system and displaced from the center the quadrupole field by $\mathbf{x}_0 = (x_0, y_0, z_0)$. The applied field then reads

$$\mathbf{B}_0 = (b_x(x + x_0), b_y(y + y_0), b_z(z + z_0)).$$

As our sphere's radius R is much larger than the expected penetration depth λ [2], we can use the approximation $\lambda/R \rightarrow 0$, i.e. we assume $\mathbf{B} = 0$ inside the sphere and $B_r = 0$ on the sphere's surface [1], where B_r denotes the radial component of the field. As there are no currents outside the sphere, there exists a scalar potential Φ s.t. $\mathbf{B} = \mathbf{B}_0 - \nabla\Phi$ and

$$\Phi = \sum_{n=0}^{\infty} r^{-(n+1)} \sum_{m=-n}^n a_{n,m} Y_n^m,$$

where $r = \sqrt{x^2 + y^2 + z^2}$ and the Y_n^m are spherical harmonics. The coefficients $a_{n,m}$ are determined by the boundary condition $B_{0,r} = (\nabla\Phi)_r$ on the sphere's surface as

$$\begin{aligned} a_{1,0} &= b_z \sqrt{\pi/3} R^3 z_0, \\ a_{1,-1} &= -\sqrt{\pi/6} R^3 (b_x x_0 + i b_y y_0), \\ a_{1,1} &= \sqrt{\pi/6} R^3 (b_x x_0 - i b_y y_0), \\ a_{2,0} &= b_z \sqrt{4\pi/45} R^5, \\ a_{2,-2} &= (b_x - b_y) \sqrt{2\pi/135} R^5, \\ a_{2,2} &= a_{2,-2}, \end{aligned}$$

all other coefficients are zero. From this field distribution we obtain the force on the sphere as

$$\mathbf{F} = -\frac{3V}{2\mu_0} (b_x^2 x_0, b_y^2 y_0, b_z^2 z_0),$$

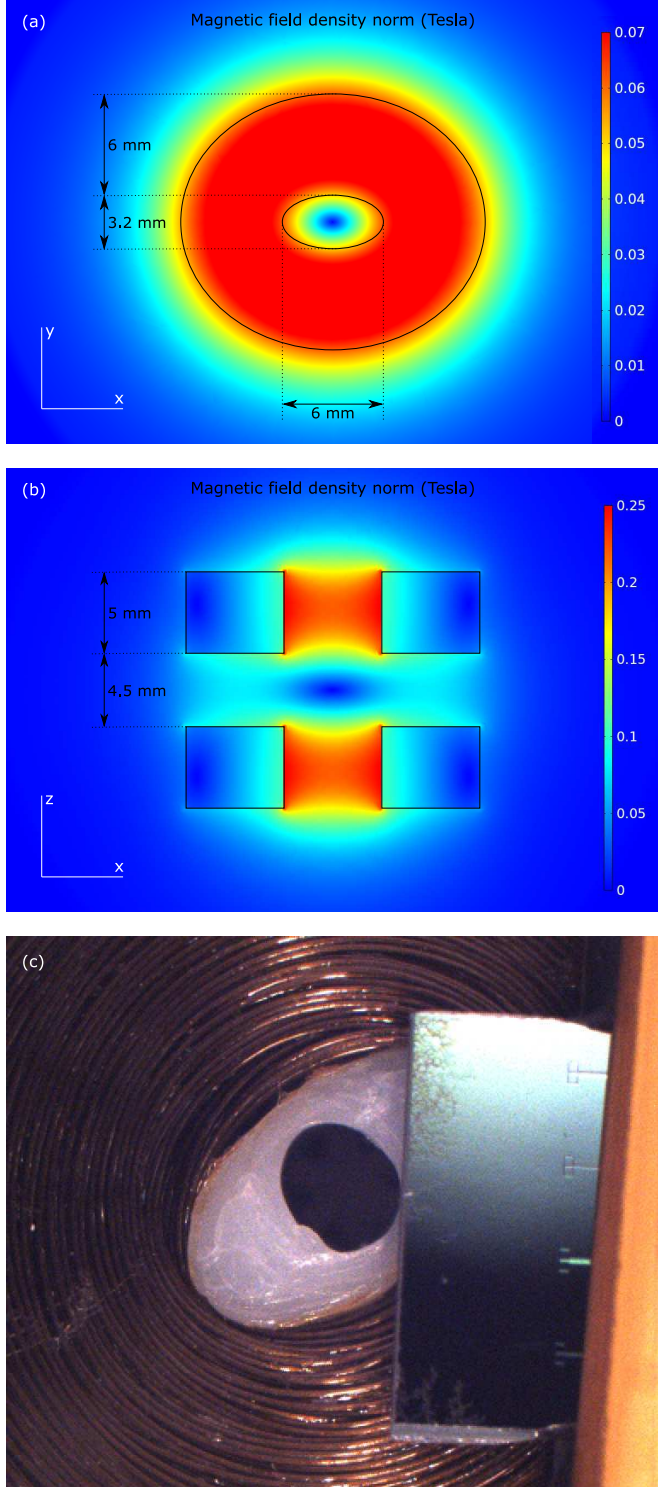


FIG. 1. (a,b)Numerical simulations of the magnetic field density created by coaxial elliptical coils with counter-propagating currents. (c)Photograph of the top surface of a single trap coil. On the right side the wafer with the pickup loops is visible (not in its final position).

where V is the volume of the sphere. The magnetic field thus creates a harmonic trapping potential for a superconducting sphere, with trapping frequencies described by

$$f_i = \sqrt{\frac{3}{8\pi^2\mu_0\rho}}|b_i|.$$

Coupling strength

The linear coupling strength with respect to a pickup loop that is described by a closed path γ is defined as $\nu_i = \partial_i\Phi_\gamma$, where Φ_γ is the flux through the area enclosed by the pickup loop and $i \in \{x_0, y_0, z_0\}$. We can express this as

$$\nu_i = \int_\gamma d\gamma \partial_i \mathbf{A}, \quad (1)$$

where \mathbf{A} denotes the magnetic vector potential, defined by $\nabla \times \mathbf{A} = \mathbf{B}$ and $\nabla \mathbf{A} = 0$. While the resulting expressions are generally bulky, they can be easily evaluated using a computer algebra system, we use WOLFRAM MATHEMATICA. We measure the current that is induced in the pickup loop using a SQUID current sensor, i.e. the pickup loop is connected to an input coil on the same wafer as the SQUID and inductively coupled to the SQUID. The coupling strength with respect to the SQUID is thus obtained as $\eta_i = \nu_i M/L$, where L is the inductance of the circuit formed by pickup loop, input coil of the current sensor, and the connecting wires, while M is the mutual inductance between input coil and SQUID. In our case $M/L \approx 0.02$. In Fig. 2 we plot the dependence of the coupling strength on the vertical separation between trap center and pickup loop, when the x- and y-position of the pickup loop relative to the trap center (as shown in the inset) is approximately the same as what we estimate for our setup (from pictures taken at room temperature, cf. Fig. 1c). The horizontal dotted lines correspond to the measured coupling strengths, while the vertical dotted line corresponds to the vertical separation extracted from camera images (approx. 400 μ m) of the levitated sphere.

Trap displacement due to gravity

The rest position of the sphere is slightly displaced from the field minimum due to gravity. In our case the setup is aligned such that the direction of gravity coincides with the z-axis. The expected displacement is thus

$$z_g = -g/(2\pi f_z)^2,$$

where $g \approx 9.81 \text{ m/s}^2$. In general this displacement needs to be taken into account when calculating the coupling

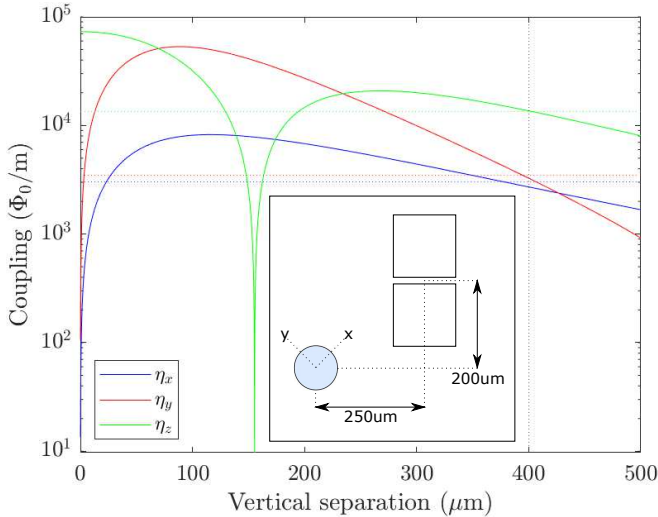


FIG. 2. Dependence of the coupling strength on the vertical separation between trap center and pickup loop, when the separation along x and y is as shown in the inset - these are the values we estimate for our setup. The vertical separation in our setup is approximately 400 μ meter. The dotted horizontal lines correspond to the measured coupling strengths.

strength, but for larger trapping frequencies it becomes negligible. We usually operate at $f_z > 200$ Hz, for which $z_g < 6 \mu\text{m}$.

CURRENT FLUCTUATIONS

Since the sphere's motional frequencies depend linearly on the trap current, current fluctuations result in frequency fluctuations, and thus can cause heating as well as broadening of the mechanical spectral peaks. We stabilize the trap current both passively and actively, as described in the following. We implement a first-order low-pass RL-filter by adding a short copper wire (resistance R_C) in parallel to the trap coils (inductance L_C). We characterize the filter's cut-off frequency by measuring its step response in an empty trap (Fig. 3). The cutoff frequency is $R_C/L_C \approx 0.036 \text{ s}^{-1}$, which results in an attenuation of approximately -180 dB at 200 Hz, while the added thermal current noise from the copper wire is only on the order of $1 \times 10^{-11} \text{ A}/\sqrt{\text{Hz}}$.

We actively stabilize the filtered trap current by monitoring the mean current source output using a digital ammeter and updating the current source output based on an estimation of the trap current. This lessens current drifts and the associated resonance broadening, as seen by comparing Fig. 4(a) with (b). Even with active current stabilization we observe drifts of the particle's resonance frequency shown in Fig. 4(d), which we attribute to low-frequency noise in the ammeter reading.

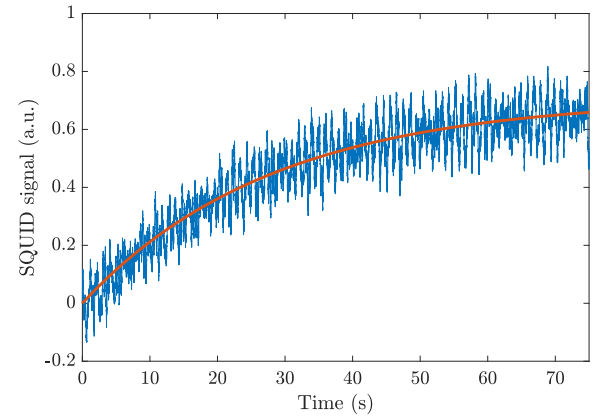


FIG. 3. Step response of the filter measured using the SQUID. The solid line is a fit of the filter's step response $1 - \exp(-R_C/L_C t)$.

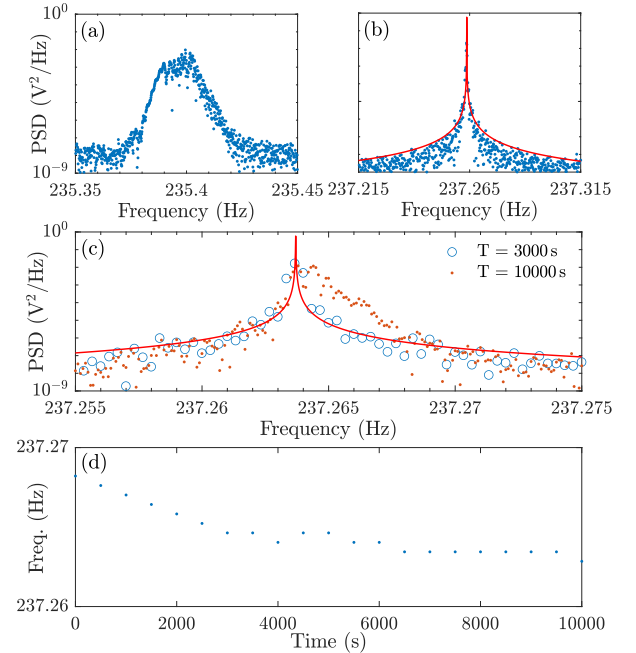


FIG. 4. (a) Typical motional resonance without active current stabilization. (b) Typical motional resonance with active current stabilization. (c) Comparison of PSDs for different measurement lengths T with trap current feedback on. For short T the linewidth is determined by the spectral resolution $1/T$ and spectral leakage, while for longer T there is still linewidth broadening due to drifts in frequency. The solid line in (b) and (c) is a Lorentzian with the linewidth set by a ringdown measurement. (d) The resonance frequency drifts by around 5 mHz over three hours.

SENSING

Taking into account measurement noise, we can calculate the force sensitivity as

$$\sqrt{S_{FF}} = \sqrt{4k_B T_0 m \gamma + |\chi|^{-2} S_{nn}},$$

where $\sqrt{S_{nn}} \approx 1 \times 10^{-9} \text{ m}/\sqrt{\text{Hz}}$ is the measurement noise and $\chi(\omega) = 1/[m(\omega_0^2 - \omega^2 - i\gamma\omega)]$ denotes the mechanical susceptibility. In our case, using $Q = 2.6 \times 10^7$ at 212 Hz and $T_0 = 15 \text{ mK}$, this would result in a force sensitivity of $\sqrt{S_{FF}} = 6.3 \times 10^{-19} \text{ N}/\sqrt{\text{Hz}}$ on resonance, close to the thermal limit of $4.9 \times 10^{-19} \text{ N}/\sqrt{\text{Hz}}$, and a noise equivalent temperature of $T_n = T_0 + |\chi(\omega_0)|^{-2} S_{nn}/(4k_B m \gamma) = 24 \text{ mK}$ (cf. Fig. 5). However, due to the stochastic fre-

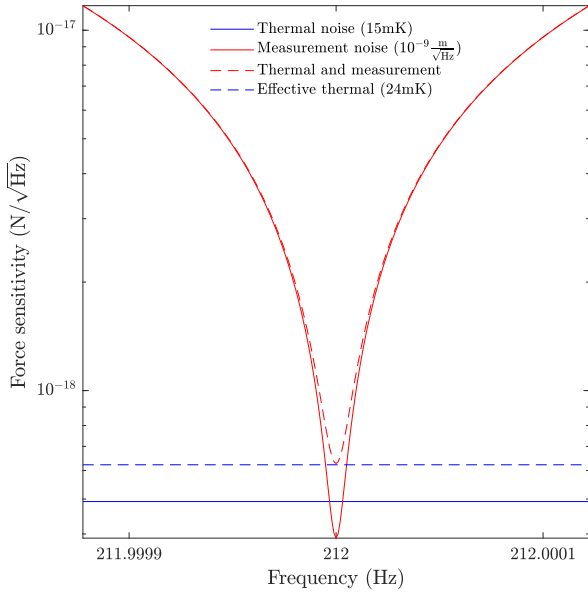


FIG. 5. (a) Force sensitivity limits due to thermal noise and measurement noise. The parameters used for the plot are $Q = 2.6 \times 10^7$ and $f_0 = 212 \text{ Hz}$.

quency fluctuations described in the last section the susceptibility is stochastic as well. We briefly sketch how this reduces our sensitivity: Note that a measurement with frequency drifts can be approximated as a series of shorter measurements at different, but constant, resonance frequencies. For a finite measurement duration T the measured force power spectral density at resonance is approximately

$$4k_B T_0 m \gamma + S_{nn} \frac{\Delta f}{\int_{\Delta f} df |\chi(f)|^2},$$

where the integration runs over the bin width $\Delta f = \frac{1}{T}$ of the bin containing the resonance. Our force sensitivity thus becomes $\sqrt{S_{FF}} = \sqrt{4k_B T_0 m \gamma + |\chi|_{avg}^{-2} S_{nn}}$ with $|\chi|_{avg}^2 = \frac{1}{\Delta f} \int_{\Delta f} df |\chi(f)|^2$. For $\Delta f > \frac{\gamma}{2\pi}$, we get $|\chi(f_0)|^2 \propto \frac{\Delta f}{\gamma}$. In our case this boosts the measurement noise above the thermal noise and, for a typical measurement, our force sensitivity decreases by at least an order of magnitude. Both improving the coupling, which corresponds to an effective decrease of the measurement noise,

and improving the stability of the resonance frequency will allow us to perform measurements limited by thermal noise. We show below that we can increase the coupling by almost four orders of magnitude. Regarding the latter, we note that persistent current coils have reached a relative current stability better than $2 \times 10^{-11}/\text{h}$ [3].

CHARACTERIZATION OF THE VIBRATION ISOLATION SYSTEM

Our vibration isolation system consists of several cylindrical plates connected by straight wires, with the top plate mounted to the 4K-platform of the dilution refrigerator and the bottom plate mounted to the aluminum can containing the magnetic trap. Electrical and thermal connections going to the setup are loosely coiled up and guided to the setup via a separate vibration isolation stage hung from the Mixing Chamber platform (cf. Fig. 6). We first characterized a single stage at room temperature, by exciting it mechanically and recording its motion with a camera. We find that the horizontal and vertical resonance frequencies are $f_h = 1.1 \text{ Hz}$ and $f_v = 18.7 \text{ Hz}$, respectively, while the librational resonance frequencies are $f_{l,1} = 0.6 \text{ Hz}$ (around vertical axis), $f_{l,2} = 8.7 \text{ Hz}$ and $f_{l,3} = 9.0 \text{ Hz}$ (around horizontal axes). We are thus limited by vertical vibrations, which in general couple to the other degrees of freedom as well [4]. We then assembled the setup as shown in Fig. 6, with the bottom plate mounted to an accelerometer (instead of the setup) used to measure acceleration along the vertical axis. The mass of the bottom plate (including the accelerometer) was 0.29 kg in this assembly. The intermediate stages are each supported by three wires of equal length, while the bottom stage is supported by a single wire. The wires are made from type 304 stainless steel with a diameter of $D = 38 \mu\text{m}$ and a yield load of 0.37 kg, as specified by the manufacturer (Fort Wayne Metals). The wires are connected to the stages with clamping connections. The vertical spring constant for the i -th stage is given by $k_{v,i} = (N_i Y D^2 \pi)/(4L_i)$, s.t. $f_{v,i} = 1/(2\pi)\sqrt{k_{v,i}/m_i}$ is the resonance frequency of a single stage. Here Y is the Young's modulus, N_i the number of supporting wires, L_i the wire length and m_i the mass of the stage. The normal mode frequencies $f_{n,i}$ of the assembled system are obtained by solving the characteristic equation of the system [4], resulting in the transfer function

$$\prod_{i=1}^3 \frac{f_{v,i}^2}{|f_{n,i}^2 - f^2|}. \quad (2)$$

In Fig. 7 we compare the vibrations measured without vibration isolation (with the accelerometer mounted to the Mixing Chamber stage of the dilution fridge) and with vibration isolation. The highest normal mode frequency

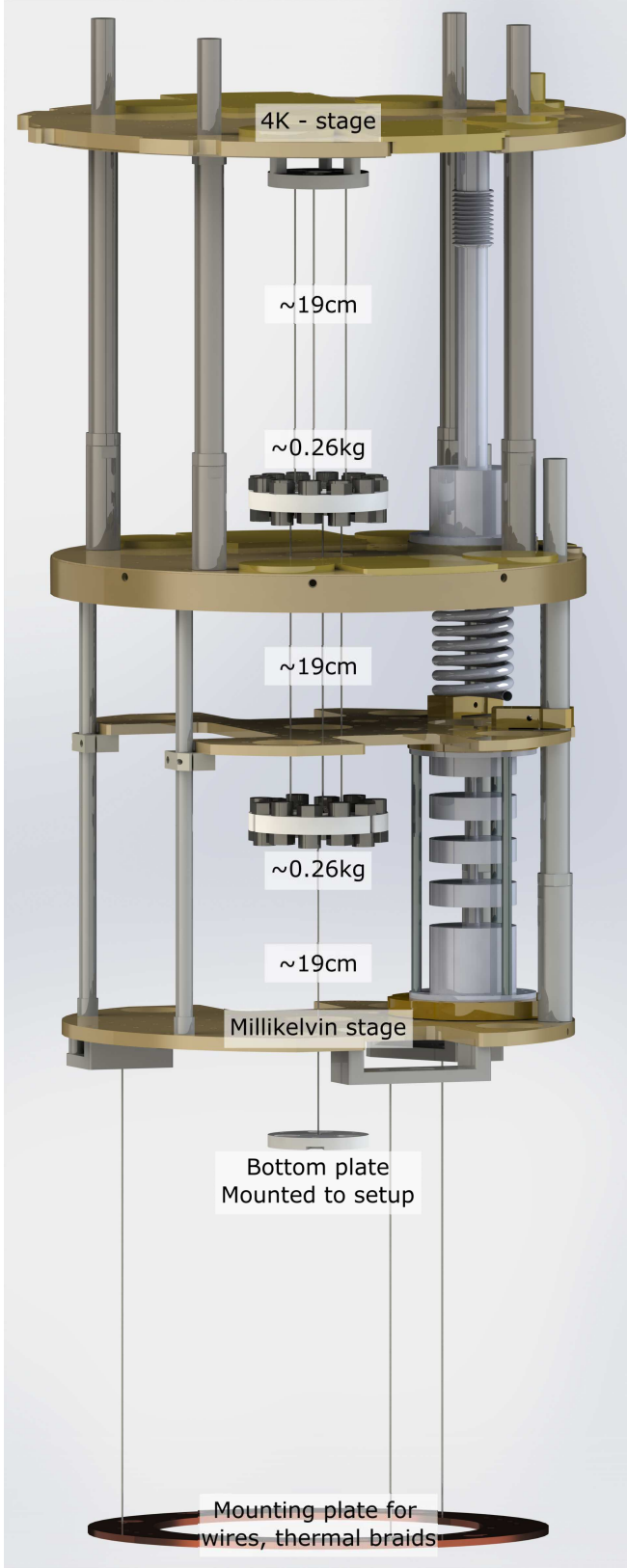


FIG. 6. Model of the vibration isolation system.

is approximately 30 Hz, above which the measured ac-

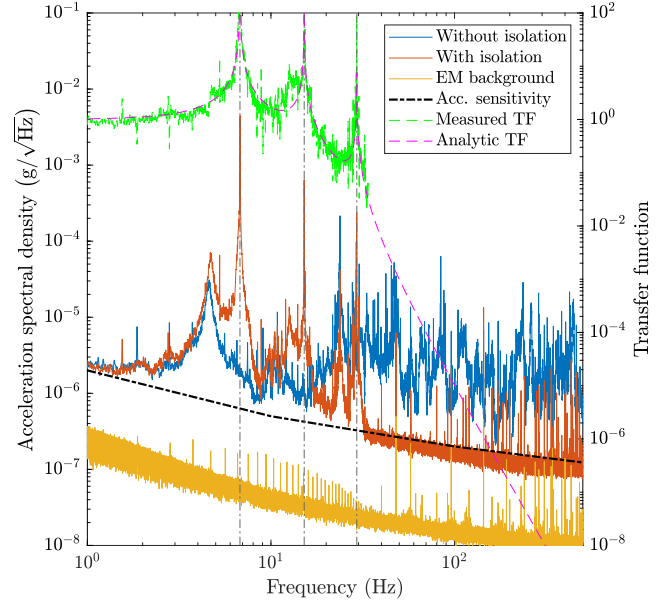


FIG. 7. Characterization of the vibration isolation. The dash-dotted black line is the sensitivity of the accelerometer, as specified by the manufacturer. The solid orange and blue lines correspond to the measured acceleration with and without the vibration isolation, respectively, while the solid yellow line is data recorded with a $1\text{ M}\Omega$ resistor connected to the SMA port inside the fridge. The dashed pink line is the analytic transfer function (Eq. 2), while the dashed green line is the measured transfer function, i.e. the ratio of the measured accelerations. The horizontal lines correspond to the normal mode resonance frequencies.

celerations quickly drop below the sensitivity of the accelerometer, when it is mounted to the vibration isolation system. At lower frequencies the measured transfer function corresponds very well to the analytical values and we use the analytic expression to extrapolate the attenuation at higher frequencies, resulting in an attenuation of 1×10^{-5} at 100 Hz and 1.5×10^{-7} at 200 Hz. The peaks at higher frequencies correspond to the electromagnetic background in the lab, which is verified by an independent measurement in which the accelerometer is replaced by an $1\text{ M}\Omega$ resistor inside the fridge. This measurement reproduces the peaks at precisely the same frequencies as in the accelerometer measurement, although with a lower magnitude - this we attribute to the additional (unshielded) wiring going from the SMA port to the accelerometer, which can act as an antenna. In an initial approach we used different masses and wire lengths, such that the attenuation was approximately 5 orders of magnitude at 200 Hz.

QUALITY FACTOR

In this section we estimate contributions to the dissipation due to gas damping and eddy currents. We also consider dissipation in the SQUID and flux creep in the pickup loop, which we rule out experimentally.

Collisions with background gas result in an additional damping of [5]

$$\gamma = \beta \frac{P}{\rho R v_{th}},$$

where $\beta \approx 1.8$ and v_{th} is the mean thermal velocity of the molecules. We do not have a direct measure of the pressure at the trap location, but we can use the measured pressure at the room temperature side of the vacuum can, $P \approx 1 \times 10^{-6}$ mbar, to set an upper limit for the expected damping. Assuming the background gas consists mostly of Helium, we get $\gamma_P \approx 3 \times 10^{-7}$ s⁻¹, two orders of magnitude below the measured damping rates.

We avoid eddy current damping by not placing any normal conductors within the inner shield. Eddy currents can still be induced in conductors outside the shield, either via openings in the shield or via the pickup circuit, part of which is placed outside the shield. In the first case, we can estimate possible eddy current losses by imagining a conductive loop with resistance R_o and inductance L_o placed around the openings in the shield. The dissipation in mode $i \in \{x_0, y_0, z_0\}$ then takes a maximum value for $R_o = 2\pi f_i L_o$, corresponding to a damping

$$\gamma_i = \frac{(\partial_i \phi)^2}{2\pi m f_i L_o}.$$

Here ϕ denotes the flux in the loop induced by the oscillation of the sphere, which can be calculated from Eq. 1. Using the dimensions of our windows and estimating $L_l > 10$ nH for a similarly sized conductive loop, we get $\gamma_i < 1 \times 10^{-9}$ s⁻¹ for all modes.

We now consider eddy current damping mediated by the pickup circuit or damping due to flux creep in the pickup circuit, as well as dissipation in the SQUID due to a real part in the SQUID input impedance [6]. This implies $\gamma_i \propto \nu_i^2$, while in the experiment the damping is approximately equal for all three COM modes. In addition, during initial measurements the pickup loop was positioned farther from the trap center and coupling strengths were approximately one order of magnitude lower than the ones reported here, but we did not see any change in the quality factor.

CALIBRATION

Our optical readout scheme is shown schematically in Fig. 8. The light source (Leica CLS150) produces a beam

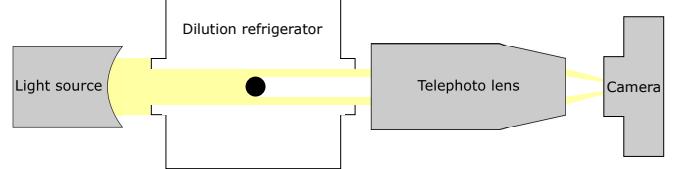


FIG. 8. Sketch of the optical setup.

of light, which is further collimated by small windows in the cryostat and the magnetic shields. After passing through the cryostat, the light is focused by a teleobjective into the camera (DFK 33UX287). Any object in the light path thus appears as a shadow on a bright background, corresponding to the projection of the object onto the image sensor. We use a frame rate of 596fps and 0.5ms exposure time to record the videos and then process them as follows. Each frame is first converted to grayscale, smoothed with Gaussian blurring, thresholded and then analyzed using the particle tracking software TRACKPY [7]. This results in datasets for the horizontal and vertical (as defined by the camera's orientation) position of the sphere. The camera is aligned such that the vertical axis is along the trap coil axis and the direction of the particle's z-motion, while the particle's motion along x and y is projected onto the camera's horizontal axis. The trap coils are aligned such that the elliptic axes are at around 45° to the optical axis, so both the x and y motion can be imaged. To get separate trajectories for each mode we implement a digital bandpass filter around the respective resonance frequency. Calibration of the sphere's displacement relies on knowledge of the optical system's magnification, which we determine using knowledge of the sphere's size (100(6) μm, as specified by the manufacturer). Including the uncertainty from the alignment of the trap coils with respect to the optical axis in addition to the ±6 % uncertainty from the size of the sphere, we estimate a total uncertainty of ±13 % for the calibrated COM displacement.

The light source is turned on only for calibration measurements, as the illumination heats the particle and limits the levitation time to approximately one hour. Further, optical band-pass filters (approximately 400 nm – 650 nm) on the millikelvin stage reduce ambient light reaching the particle and heating it. Without the filters (and the light source turned off) levitation times are limited to around four hours, while we have not yet found a limit (>30 h) using the filters.

OPTIMIZATIONS AND GROUND STATE COOLING

In this section we provide more detail on how to implement the improvements that are necessary to per-

form feedback cooling to the ground state. We will consider only cooling of the z-mode, cooling of the other modes and 3D-cooling can be characterized and optimized in an analogous manner. We first show that the coupling strength can be increased by almost four orders of magnitude, s.t. the measurement noise (in units of $\text{m}/\sqrt{\text{Hz}}$) with a state-of-the-art SQUID decreases to $1 \times 10^{-15} \text{ m}/\sqrt{\text{Hz}}$. We then take into account the back action from the SQUID due to the circulating current and determine the standard quantum limit (SQL) of our system. We proceed to evaluate the requirements for ground state cooling as well as contributions to heating from vibrations and frequency fluctuations.

Coupling strength

We can increase the coupling strength by better positioning of the pickup loop relative to the superconducting sphere and by increasing the number of turns of the pickup loop, thus matching its inductance to that of the input coil. For the calculation, we will assume a planar pickup loop with circular windings, positioned coaxial with the z-axis. Then Eq. 1 leads to

$$\nu_1 = \pi b_z R_P^2 \left(\frac{R^2}{R_P^2 + Z_P^2} \right)^{\frac{3}{2}} \times \left(1 - \frac{R^2}{R_P^2 + Z_P^2} \left(1 - \frac{5Z_P^2}{R_P^2 + Z_P^2} \right) \right) \quad (3)$$

for the coupling strength w.r.t. a single turn of the pickup loop with radius R_P and z-position Z_P . The coupling strength to a multi-turn pickup loop can be written as a sum of terms of this form, $\nu = \sum_i \nu_1(R_{P,i}, Z_{P,i})$, and the coupling strength to the SQUID (cf. Fig. 9) is obtained as

$$\eta = \nu \frac{k \sqrt{L_I L_S}}{L_P + L_I + L_W}.$$

Here L_P , L_I and L_S are the inductances of pickup coil, SQUID input coil and SQUID, respectively. We have used that the the mutual inductance M between input coil and SQUID can be written as $M = k \sqrt{L_I L_S}$ with $|k| < 1$. L_W denotes the stray inductance of the pickup circuit and is in our case dominated by the wires connecting the pickup coil to the SQUID, $L_W \approx 100 \text{ nH}$.

A relevant figure of merit for the measurement noise of the SQUID is the so-called energy resolution $S_{EE} = \frac{S_{\phi\phi}}{2L_S}$, with state-of-the-art SQUIDs reaching values on the order of \hbar [8, 9]. In terms of position resolution this can be written as

$$S_{nn} = \frac{S_{\phi\phi}}{\eta^2} = \frac{2S_{EE}}{k^2} \frac{(L_P + L_I + L_W)^2}{\nu^2 L_I}. \quad (4)$$

In order to get a realistic estimate for this we will use the SQUID parameters presented in [9], i.e. $L_S = 15 \text{ pH}$,

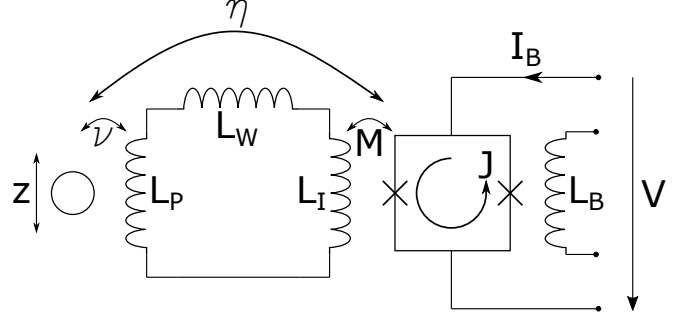


FIG. 9. Schematic of the readout circuit. The working point of the SQUID is set by the bias current I_B and the bias flux coupled into the SQUID via L_B . For appropriate bias values and small changes in flux (in FLL mode this is assured by applying feedback over L_B), the voltage drop V is proportional to the flux in this SQUID loop.

$L_I = 0.53 \text{ pH}$, $M = 2.3 \text{ nH}$ and $\frac{S_{\phi\phi}}{2k^2 L_S} = 5.5\hbar$. For the pickup coil we assume a wire width of $0.3 \text{ }\mu\text{m}$ and a distance between the wires of $0.45 \text{ }\mu\text{m}$, which is also the resolution of the input coil of our existing SQUID. We use the modified Wheeler formula [10] to determine L_P , s.t. we get a fully analytical expression for S_{nn} . We also restrict us to $Z_P \geq R$. Given these parameters, as well as $b_z = 147 \text{ T/m}$, we minimize S_{nn} with respect to R_P , Z_P and N , where R_P now denotes the inner radius of the pickup coil and N is the number of turns. This results in $\eta \approx 5 \times 10^7 \phi_0/\text{m}$ and $S_{nn} \approx 1 \times 10^{-15} \text{ m}$ for $Z_P = R$, $R_P \approx 0.6R$ and $N = 67$. We note that the scaling of the coupling (Eq. 3) means that the measurement noise can be further decreased by working with higher gradients or using larger particles (a scale-independent expression for the coupling is easily obtained by measuring distance in units of R , magnetic fields in units of $b_z R$ and thus the coupling in units of $b_z R^2$).

The standard quantum limit

Equation 4 for the readout signal measured with the SQUID is valid only when the back-action stemming from the circulating SQUID current onto the levitating particle is negligible. This is a reasonable assumption given the weak coupling in our current setup, but for increased coupling strength the back-action should be considered. All relevant parameters are stated for the SQUID coupled to the input circuit and can be different than the parameters of the uncoupled SQUID, depending on the capacitive coupling at the Josephson frequency [6]. The readout noise is set by the flux noise, while the back-action noise is determined by fluctuations of the circulating current J . For a shunted SQUID the origin of both flux and current fluctuations is current noise in the shunt resistors and the quantum limit that arises from

zero-point-fluctuations is $\sqrt{S_{\phi\phi}S_{JJ} - S_{\phi J}^2} \geq \hbar$ [11, 12]. We will assume in the following that correlations between flux and current noise are negligible, $S_{\phi J} \approx 0$ [12, 13].

A current J around the SQUID loop will effect a force $-\eta J$ on the levitated sphere and thus the measured displacement PSD of the sphere becomes

$$S_{zz}^m = \frac{S_{\phi\phi}}{\eta^2} + |\chi|^2(S_{FF}^{th} + \eta^2 S_{JJ}).$$

The product of measurement noise and back-action force noise thus fulfills the Heisenberg-like inequality $\frac{S_{\phi\phi}}{\eta^2} \eta^2 S_{JJ} \geq \hbar^2$ and S_{zz}^m is minimized for $\eta^2 = \frac{1}{|\chi|} \sqrt{\frac{S_{\phi\phi}}{S_{JJ}}}$, such that

$$S_{zz}^m = 2|\chi| \sqrt{S_{\phi\phi}S_{JJ}} + |\chi|^2 S_{FF}^{th}.$$

For $\sqrt{S_{\phi\phi}S_{JJ}} = \hbar$ this corresponds to the standard quantum limit.

Feedback cooling

We now assume we provide direct feedback s.t. the effective damping of the oscillator becomes $\gamma + \Gamma$, where Γ is the cold damping added by the feedback [14] and $\tilde{\chi}(\omega) = 1/[m(\omega_0^2 - \omega^2 - i(\gamma + \Gamma)\omega)]$ is the effective susceptibility. The measurement noise will also enter the feedback system, resulting in an additional force, and the displacement power spectral density becomes

$$S_{zz} = |\tilde{\chi}|^2 \left(S_{FF}^{th} + \eta^2 S_{JJ} + (m\omega\Gamma)^2 \frac{S_{\phi\phi}}{\eta^2} \right).$$

For $\Gamma = \frac{\eta^2}{m\omega_0 \tilde{L}_S} \gg \gamma$ this corresponds a mean phonon number

$$\bar{n} = \frac{1}{\hbar\eta^2} \left(2k_B T_0 m \gamma \tilde{L}_S \right) + \frac{1}{2} \left(\frac{\sqrt{S_{\phi\phi}S_{JJ}}}{\hbar} - 1 \right),$$

where we have introduced the shorthand $\tilde{L}_S = \sqrt{\frac{S_{\phi\phi}}{S_{JJ}}}$. Close to the optimum working point $\tilde{L}_S \approx L_S$ [13]. Using $\eta = 5 \times 10^7 \Phi_0/m$ as well as $T_0 = 15 \text{ mK}$, $m = 5.6 \mu\text{g}$ and $L_S = 15 \text{ pH}$, we need $\gamma \approx 1 \times 10^{-6} \text{ s}^{-1}$ to keep the left term negligible. Ground state cooling then requires $\sqrt{S_{\phi\phi}S_{JJ}} < 3\hbar$. While current noise in SQUIDs is challenging to measure [15], for $\tilde{L}_S \approx L_S$ we would expect $\sqrt{S_{\phi\phi}S_{JJ}} \approx 2S_{EE}$. The lowest energy resolution reported up to date is $S_{EE} \approx 1.7\hbar$ [8], so ground state cooling by continuous feedback will require a state-of-the-art SQUID.

Heating

We now consider fluctuations of the trap center with spectral density $S_{\epsilon\epsilon}$ as well as fractional fluctuations of

the spring constant with spectral density $S_{\delta\delta}$. We note that the heating rate $\Gamma_\delta E$ due to frequency fluctuations is proportional to the energy E of the oscillator. The average energy of the oscillator is then described by

$$\langle \dot{E} \rangle = (\Gamma_\delta - \gamma) \langle E \rangle + k_B T_0 \gamma + \dot{Q}_\epsilon,$$

where \dot{Q}_ϵ is the heating rate due to fluctuations of the trap center. For $\Gamma_\delta < \gamma$ this results in an effective temperature of

$$T_{eff} = \frac{k_B T_0 \gamma + \dot{Q}_\epsilon}{k_B (\gamma - \Gamma_\delta)}.$$

The heating rates are given by [16]

$$\dot{Q}_\epsilon = \frac{1}{4} m \omega_0^4 S_{\epsilon\epsilon}(\omega_0),$$

and

$$\Gamma_\delta = \frac{1}{4} \omega_0^2 S_{\delta\delta}(2\omega_0).$$

Using the values from the preceding paragraph, ground state cooling requires approximately $\sqrt{S_{\delta\delta}(2\omega_0)} < 1 \times 10^{-7} / \sqrt{\text{Hz}}$ and $\sqrt{S_{\epsilon\epsilon}(\omega_0)} < 1 \times 10^{-19} \text{ m} / \sqrt{\text{Hz}}$ (corresponding to $T_{eff} < 20 \text{ mK}$). Regarding the former we note that relative fluctuations on the order of one part per billion can be reached in superconducting coils [17], while the latter requires further improvements to our vibration isolation system. Suspending the system from the top plate of the cryostat would allow us to add two more stages and achieve the required vibration suppression.

* joachim.hofer@univie.ac.at

† Currently at: QuTech, Delft University of Technology, Delft, The Netherlands

- [1] J. Hofer and M. Aspelmeyer, Analytic solutions to the maxwell-london equations and levitation force for a superconducting sphere in a quadrupole field, *Physica Scripta* **94**, 125508 (2019).
- [2] J. D. Livingston, Magnetic properties of superconducting lead-base alloys, *Phys. Rev.* **129**, 1943 (1963).
- [3] R. S. Van Dyck, D. L. Farnham, S. L. Zafonte, and P. B. Schwinberg, Ultrastable superconducting magnet system for a penning trap mass spectrometer, *Review of Scientific Instruments* **70**, 1665 (1999).
- [4] T. L. Aldcroft, P. F. Michelson, R. C. Taber, and F. A. McLoughlin, Six-degree-of-freedom vibration isolation systems with application to resonant-mass gravitational radiation detectors, *Review of Scientific Instruments* **63**, 3815 (1992).
- [5] L. D. Hinkle and B. R. F. Kendall, Pressure-dependent damping of a particle levitated in vacuum, *Journal of Vacuum Science & Technology A* **8**, 2802 (1990).
- [6] J. M. Martinis and J. Clarke, Signal and noise theory for a dc squid amplifier, *Journal of Low Temperature Physics* **61**, 227 (1985).

- [7] J. C. Crocker and D. G. Grier, Methods of digital video microscopy for colloidal studies, *Journal of Colloid and Interface Science* **179**, 298 (1996).
- [8] D. D. Awschalom, J. R. Rozen, M. B. Ketchen, W. J. Gallagher, A. W. Kleinsasser, R. L. Sandstrom, and B. Bumble, Low-noise modular microsusceptometer using nearly quantum limited dc squids, *Applied Physics Letters* **53**, 2108 (1988).
- [9] P. Carelli, M. G. Castellano, G. Torrioli, and R. Leoni, Low noise multiwasher superconducting interferometer, *Applied Physics Letters* **72**, 115 (1998).
- [10] H. Wheeler, Simple inductance formulas for radio coils, *Proceedings of the Institute of Radio Engineers* **16**, 1398 (1928).
- [11] R. H. Koch, D. J. Van Harlingen, and J. Clarke, Quantum noise theory for the dc squid, *Applied Physics Letters* **38**, 380 (1981).
- [12] V. Danilov, K. Likharev, and A. Zorin, Quantum noise in squids, *IEEE Transactions on Magnetics* **19**, 572 (1983).
- [13] C. D. Tesche and J. Clarke, dc squid: Current noise, *Journal of Low Temperature Physics* **37**, 397 (1979).
- [14] T. W. Penny, A. Pontin, and P. F. Barker, Performance and limits of feedback cooling methods for levitated oscillators: A direct comparison, *Phys. Rev. A* **104**, 023502 (2021).
- [15] J. Martinis and J. Clarke, Measurements of current noise in dc squids, *IEEE Transactions on Magnetics* **19**, 446 (1983).
- [16] M. E. Gehm, K. M. O'Hara, T. A. Savard, and J. E. Thomas, Dynamics of noise-induced heating in atom traps, *Phys. Rev. A* **58**, 3914 (1998).
- [17] J. W. Britton, J. G. Bohnet, B. C. Sawyer, H. Uys, M. J. Biercuk, and J. J. Bollinger, Vibration-induced field fluctuations in a superconducting magnet, *Phys. Rev. A* **93**, 062511 (2016).